Mutations in *PMPCB* Encoding the Catalytic Subunit of the Mitochondrial Presequence Protease Cause Neurodegeneration in Early Childhood

F.-Nora Vögtle,[1,17,*] Björn Brändl,[2,17] Austin Larson,[3,17] Manuela Pendziwiat,[4,17] Marisa W. Friederich,[3,17] Susan M. White,[5,6] Alice Basinger,[7] Cansu Kücükköse,[1,8] Hiltrud Muhle,[4] Johanna A. Jähn,[4] Oliver Keminer,[9] Katherine L. Helbig,[10] Carolyn F. Delto,[11] Lisa Myketin,[1] Dirk Mossmann,[1] Nils Burger,[1] Noriko Miyake,[12] Audrey Burnett,[7] Andreas van Baalen,[4] Mark A. Lovell,[13] Naomichi Matsumoto,[12] Maie Walsh,[14] Hung-Chun Yu,[3,19] Deepali N. Shinde,[15] Ulrich Stephani,[4] Johan L.K. Van Hove,[3,18] Franz-Josef Müller,[2,16,18] and Ingo Helbig[4,10,18,*]

Mitochondrial disorders causing neurodegeneration in childhood are genetically heterogeneous, and the underlying genetic etiology remains unknown in many affected individuals. We identified biallelic variants in *PMPCB* in individuals of four families including one family with two affected siblings with neurodegeneration and cerebellar atrophy. *PMPCB* encodes the catalytic subunit of the essential mitochondrial processing protease (MPP), which is required for maturation of the majority of mitochondrial precursor proteins. Mitochondria isolated from two fibroblast cell lines and induced pluripotent stem cells derived from one affected individual and differentiated neuroepithelial stem cells showed reduced PMPCB levels and accumulation of the processing intermediate of frataxin, a sensitive substrate for MPP dysfunction. Introduction of the identified *PMPCB* variants into the homologous *S. cerevisiae* Mas1 protein resulted in a severe growth and MPP processing defect leading to the accumulation of mitochondrial precursor proteins and early impairment of the biogenesis of iron-sulfur clusters, which are indispensable for a broad range of crucial cellular functions. Analysis of biopsy materials of an affected individual revealed changes and decreased activity in iron-sulfur cluster-containing respiratory chain complexes and dysfunction of mitochondrial and cytosolic Fe-S cluster-dependent enzymes. We conclude that biallelic mutations in *PMPCB* cause defects in MPP proteolytic activity leading to dysregulation of iron-sulfur cluster biogenesis and triggering a complex neurological phenotype of neurodegeneration in early childhood.

Introduction

Mitochondria are indispensable for cellular function as these organelles are involved in many critical cellular processes. Mutations in mitochondrial or nuclear genes can cause mitochondrial diseases comprising a heterogeneous group of conditions that represent a significant proportion of complex neurological disorders of childhood, particularly conditions with a neurodegenerative course.[1–3] The vast majority of mitochondrial genes are encoded in the nuclear genome requiring a well-orchestrated import of mitochondrial preproteins after their translation on cytosolic ribosomes into the organelle.[4–7] Approximately 70% of preproteins carry N-terminal cleavable presequences that function as targeting signals for mitochondrial protein import.[8] Complex protein import machineries recognize the presequences and facilitate translocation of the precursors across the mitochondrial membranes.[4–6,9,10] The essential mitochondrial processing protease (MPP) located in the mitochondrial matrix is the key enzyme to remove these presequences to allow folding and functioning of the mature protein. MPP is highly conserved from yeast to human and consists of two subunits: the catalytic PMPCB subunit (Mas1 in yeast) and the non-catalytic PMPCA subunit (Mas2 in yeast). While PMPCB/Mas1 is a metalloprotease with a zinc-binding motif, PMPCA/Mas2 has been implicated in substrate recognition and binding.[11–15]

Here, we report on four families with five affected individuals carrying biallelic variants in *PMPCB* (MIM: 603131). All children presented with episodic neurological regression, basal ganglia lesions, and cerebellar atrophy

[1]Institute of Biochemistry and Molecular Biology, ZBMZ, Faculty of Medicine, University of Freiburg, Freiburg 79104, Germany; [2]Department of Psychiatry and Psychotherapy, University Hospital Schleswig Holstein, Kiel 24105, Germany; [3]Department of Pediatrics, Section of Clinical Genetics and Metabolism, University of Colorado, Aurora, CO 80045, USA; [4]Department of Neuropediatrics, Christian-Albrechts-University of Kiel, Kiel 24105, Germany; [5]Victorian Clinical Genetics Services, Murdoch Children's Research Institute, Melbourne, VIC 3052, Australia; [6]Department of Paediatrics, University of Melbourne, Melbourne, VIC 3052, Australia; [7]Cook Children's Physician Network, Department of Genetics, Fort Worth, TX 76102, USA; [8]Faculty of Biology, University of Freiburg, Freiburg 79104, Germany; [9]Fraunhofer-Institut für Molekularbiologie und Angewandte Ökologie IME, ScreeningPort, Hamburg 22525, Germany; [10]Division of Neurology, The Children's Hospital of Philadelphia, Philadelphia, PA 19104, USA; [11]Rudolf Virchow Center for Experimental Biomedicine, University of Würzburg, Würzburg 97080, Germany; [12]Department of Human Genetics, Yokohama City University Graduate School of Medicine, Yokohama 236-0004, Japan; [13]Department of Pathology, University of Colorado, Aurora, CO 80045, USA; [14]Adult Genetic Medicine, Royal Melbourne Hospital, Melbourne, VIC 3052, Australia; [15]Division of Clinical Genomics, Ambry Genetics, Aliso Viejo, CA 92656, USA; [16]Max Planck Institute for Molecular Genetics, Berlin 14195, Germany
[17]These authors contributed equally to this work
[18]These authors contributed equally to this work
[19]Present address: Human Longevity, Inc., San Diego, CA 92121, USA
*Correspondence: nora.voegtle@biochemie.uni-freiburg.de (F.-N.V.), helbigi@email.chop.edu (I.H.)
https://doi.org/10.1016/j.ajhg.2018.02.014.

and were suspected of having a mitochondrial disorder. Analysis of human induced pluripotent stem cells (hiPSCs) derived from one of the affected individuals and neuroepithelial stem cells (NESs) differentiated thereof, fibroblasts as well as functional studies in yeast bearing the affected individuals' variants in the homologous Mas1 protein demonstrate that the identified *PMPCB* variants severely impair mitochondrial presequence processing. Furthermore, the yeast model revealed significant defects in the mitochondrial biosynthesis of iron-sulfur clusters, which are indispensable for many cellular functions including mitochondrial bioenergetic processes, nuclear genome maintenance, and cytosolic protein translation. Analysis of biopsied material from an affected individual identified changes in the formation and decreased activity of respiratory chain complexes, which have several Fe-S clusters incorporated, and dysfunction of the iron-sulfur cluster containing aconitase enzyme localized in mitochondria and the cytosol. We identify disease-causing mutations in *PMPCB* as a new mechanism in mitochondrial disease triggering a Leigh-like phenotype with cerebellar atrophy in early childhood.

Subjects and Methods

Subject Evaluation

Informed consent for participation in this study was obtained from all parents in agreement with the Declaration of Helsinki. All studies were completed per protocol with local approval by institutional review boards (IRB). All families underwent detailed review of clinical data for study inclusion.

Family A was evaluated at the Mitochondrial Clinic of Children's Hospital Colorado, Aurora, USA and consented on IRB-approved studies (COMIRB 07-0386 and 16-0146). Family B was evaluated at the Department of Genetics at Cook Children's Physician Network in Fort Worth, Texas, USA, and enrolled through a research protocol at the Children's Hospital of Philadelphia. Family C was evaluated at the Victorian Clinical Genetics Services, Murdoch Children's Research Institute, and the study was approved by the local institutional ethics committees at the Royal Children's Hospital, Melbourne, Australia, and Yokohama City University Faculty of Medicine, Yokohama, Japan. Family D was evaluated at the Department of Neuropediatrics, University of Kiel, Germany, in the setting of the EuroEPINOMICS project on Rare Epilepsy Syndromes (RES) and a Trilateral Project German-Israeli-Palestinian project by the German Research Foundation. The EuroEPINOMICS study and the Trilateral project (A 115/02, A 116/02) as well as the protocol for the generation of hiPSCs at the Zentrum für Integrative Psychiatrie at the University Hospital Schleswig-Holstein were approved by the local institutional review board of the University Kiel (A 145/11). The GeneMatcher tool was used to search and identify additional individuals with *PMPCB* variants as the suspected diagnosis.[16]

Genetic Analysis

Family A

Trio-based whole-exome sequencing (WES) was performed by the Medical College of Wisconsin (Milwaukee, WI). Targeted enrichment used the Agilent All Exon Kit, v.4. Sequencing was performed on an Illumina HiSeq 2500 per manufacturer protocols. Reads were mapped to the reference human genome (GRCh37/hg19) using Burrows-Wheeler Aligner (BWA).[17] Variants were called using SAMtools[18] and further annotated using SeattleSeq. Filtering and test of inheritance model were done using Galaxy.[19] Variants were filtered against dbSNP build 137, 1000 Genomes (November 23, 2010 release version), Exome Variant Server (EVS, ESP6500SI-V2), and Exome Aggregation Consortium ExAC browser (v.0.3). Rare variants were identified with minor allele frequency less than 1% using dbSNP137. The sequence data from the family were then used to test for causal variants under different inheritance models. The *PMPCB* variants were verified by Sanger sequencing.

Family B

Trio-based WES was performed by a commercial laboratory (Ambry Genetics) as previously described.[20,21] In brief, samples were prepared with the IDT xGen Exome Research Panel V1.0 (IDT) and sequenced using paired-end, 100-cycle chemistry on the Illumina HiSeq 2500 platform (Illumina). Sequences were aligned to GRCh37/hg19 and variant calls were generated using CASAVA and Pindel. After removal of common single-nucleotide polymorphisms (SNP), intergenic and 3′/5′ UTR variants, non-splice-related intronic variants, and synonymous variants, the remaining variants were filtered for *de novo* dominant and homozygous and compound heterozygous recessive inheritance models. Except for the variants in *PMPCB*, no other pathogenic or likely pathogenic variants were identified in the family.

Family C

Trio-based WES was performed using previously published methods.[22,23] In brief, genome partitioning was performed with SureSelect Human All Exon V5 (for affected individual) or V6 (for parents) (Agilent Technologies). The prepared libraries were run on HiSeq 2000/2500 (Illumina). Sequences were aligned to GRCh37/hg19 by NovoAlign. After PCR duplication by Picard Tools, variant calling and annotation were performed by Genome Analysis Toolkit and ANNOVAR.[24] The candidate variants were highlighted based on autosomal- or X-linked-dominant (*de novo*) and autosomal-recessive inheritance models. The candidate variants were validated by trio-based Sanger sequencing.

Family D

WES was performed for individual D:II-1 and her parents as reported previously[25] and the affected brother (D:II-2) separately. WES was performed at Wellcome Trust Sanger Institute (Hinxton, Cambridgeshire) as part of the EuroEPINOMICS RES project using the Illumina TruSeq DNA Sample Preparation Kit, the Agilent Technologies SureSelect Human All Exon 50Mb Kit, and the Illumina HiSeq2000 as per manufacturer's protocols. Sequencing of individual D:II-2 was performed at the University of Kiel using the TruSeq DNA Sample Preparation Kit and the Illumina HiSeq2000. Sequencing reads of all samples passing quality filtering were aligned to the GRCh37/hg19 human reference genome with the Burrows-Wheeler Aligner, marking of duplicate reads was performed using Picard. Variant calling was performed using the GATK 3.7 Haplotype caller, annotation of VCF files was performed using ANNOVAR.[24] Custom tools were used for the identification of potentially causative variants under various inheritance models. Other than the homozygous *PMPCB* variant in both siblings, no further candidates were identified under various inheritance models. The *PMPCB* variant was confirmed using Sanger sequencing.

Structural Modeling

The *PMPCB* variants identified in the affected individuals were modeled into the crystal structure of yeast MPP in complex with

the cytochrome C oxidase IV presequence peptide[11] (PDB: 1hr8). Mutations were introduced *in silico* and side chains positioned in preferred rotamer conformations while minimizing steric overlaps and optimizing hydrogen-bonding capabilities using the software Coot.[26] Images were made using The PyMOL Molecular Graphics System, v1.8 Schrödinger, LLC.

hiPSC Generation and Cell Culture

Human dermal fibroblast cells (HDF) were obtained from individual D:II-2 and both parents using a 3 mm punch biopsy. Biopsy material was segmented into smaller fragments, fixed onto tissue culture-treated plastic dishes, and maintained in HDF medium containing DMEM Glutamax, 1% penicillin/streptomycin, and 20% fetal calf serum (FCS) at 37°C and 5% CO_2. HDF medium was changed every other day to obtain a 90% confluent monolayer until the cells were passaged at a 1:3 ratio using trypsin. Control C1, human embryonic stem cell line (hESC) WA09 (WA1009-A), was purchased from the WiCell Research Institute (Madison, WI) under permission of the Robert Koch Institute (AZ 1710-79-1-4-42). Control C2, cell line ZIPi013-A-2 was reprogrammed from the neonatal fibroblast line HDF51 obtained from The Scripps Research Institute (La Jolla, CA) yielding the control cell lines C2.2 and C2.5. The parental control HDF line and other hiPSC lines derived thereof have been whole-genome sequenced and no variants in *PMPCB* were reported.[27] The WA09 cell line has been subjected to WES, most recently by Merkle et al.,[28] and no *PMPCB* mutations were reported. All cell lines were routinely tested for mycoplasma contamination (Universal Mycoplasma Detection Kit, ATCC). Pluripotent stem cell lines were induced from control HDF and individual D:II-2 (yielding the *PMPCB* cell lines D:II-2.4, D:II-2.9, D:II-2.11) using episomal plasmids following a published protocol with minor modification.[29] All plasmids were a gift by Shinya Yamanaka and obtained via Addgene. Briefly, 2 μg of pCXLE-hSK (#27080), pCXLE-hUL (#27078), and pCXLE-hOCT3/4-shp53F (#27077) were transfected into 1×10^6 HDF using the Neon microporator device with 100 μL electroporation tips (settings: 1.650 V, 10 ms, 3 timed pulses, Thermo Fisher Scientific) according to the manufacturer's protocol. Transfected cells were resuspended in 10 mL fibroblast medium containing 90% 1 × MEM (Thermo Fisher Scientific) supplemented with 10% FCS and 2.5×10^4 HDF/cm^2 were reseeded onto Matrigel-coated (0.5 mg/mL) six-well plates. 2 days post transfection, fibroblast medium was replaced with TeSR-E7 (StemCell Technologies, Inc.) and cells were fed every other day with 2 mL TeSR-E7/well. On day 26–30 post transfection, emerging hiPSC colonies were picked and transferred onto Matrigel-coated plastic dishes (Corning; 0.5 mg/mL) in TeSR-E8 medium (StemCell Technologies, Inc.) for further expansion. hESCs were cultured under the same conditions. Enzyme-free colony expansion using EDTA was performed every 3–4 days at a 1:6 ratio based on a protocol previously described.[30]

For confirming the pluripotent status, immunocytochemical (ICC) staining for pluripotency markers[31] and PluriTest[32] was performed. Cells were seeded as single cells on 96-well plates (1×10^4 cells/well) and after 48 hr fixed for 15 min with 4% paraformaldehyde and incubated in blocking buffer (5% FCS, 95% 1× PBS, 0.3% Triton X-100) for 1 hr. Samples were incubated in primary antibody dilution (see Table S1 for details) overnight at 4°C. Cells were washed with 1× PBS, incubated with 1:1,000 diluted AlexaFluor 488 secondary antibody (Thermo Fisher Scientific) in blocking buffer for 2 hr at room temperature, and washed and images were obtained using an Opera imaging device (PerkinElmer). Additionally, pellets with 1–1.5 × 10^6 cells were harvested and snap frozen in liquid nitrogen for PluriTest analysis. Samples were processed at AROS Applied Biotechnology A/S (Denmark) for RNA isolation and analyzed with Illumina HT-12 v4 microarrays following the manufacturer's instructions (Illumina). Raw data files were processed as previously described.[32] All hiPSC clones were carried out between passage 18 to 20 using standard G-banding (Institute for Human Genetics Hamburg-Eppendorf). Karyotyping was performed on at least 20 metaphases per sample.

Neural Differentiation and Characterization of NES

Differentiation of hiPSCs/hESCs toward neuroepithelial stem cells (NES) was performed based on previously published protocols with minor modifications.[33–35] Undifferentiated hiPSCs/hESCs with 70% to 80% confluence were washed once with 1× DPBS and briefly detached with Accutase (Thermo Fisher Scientific). Solution was neutralized using TesR-E8 and cells were centrifuged at 200 × *g* for 3 min. Cells were resuspended in fresh TeSR-E8 supplemented with 0.5 μM Thiazovivin (Tocris Bioscience) with subsequent seeding (2×10^5 cells/cm^2) onto Matrigel-coated (1 mg/mL) six-well plates to form a confluent monolayer. Medium was changed 24 hr post seeding to neural induction medium (NIM) containing 50% 1× DMEM/F-12, 50% 1× Neurobasal Medium, 1:200 N2 supplement (100×), 1:100 B-27 supplement (50×) (all GIBCO), 1.6 g/L D-Glucose, 2 μM XAV939 (Sigma-Aldrich), 500 nM A-83-01, and 200 nM LDN193189 (both Stemgent) with daily medium change. On day 10 neuronal cultures were preincubated with 0.5 μM Thiazovivin for 1 hr and washed once with 1× DPBS. Cells were detached with 1× TrypLE Select (Thermo Fisher Scientific) for 8 to 12 min at 37°C and resuspended in NIM following centrifugation at 200 × *g* for 3 min. The cell pellet was resuspended in NES neural expansion medium (NEM) containing 50% 1× DMEM/F-12, 50% 1× Neurobasal Medium, 1:200 N2 supplement (100×), 1:100 B-27 supplement (50×), 1.6 g/L D-Glucose, 10 ng/mL hrFGF basic, and 10 ng/mL hrEGF (both R&D Systems). NES were seeded on growth factor reduced Matrigel (Corning)-coated six-well plates for further expansion with high cell densities (1:1.5 to 1:2 ratio) in NEM supplemented with 0.5 μM Purmorphamine (Sigma-Aldrich) and 0.5 μM Thiazovivin. Cells were cultured in NEM medium for additional 4 days and harvested with 1× TrypLE Select for subsequent isolation of mitochondria. For immunocytochemical characterization, NES were seeded (1.7×10^5 cells/well) onto Matrigel-coated 96-well plates (PerkinElmer) and cultured for another 4 days in NEM.

Staining and Quantitative Imaging

Standard staining immunofluorescence protocols were applied. In short, cells were washed with PBS and permeabilized for 10 min in PBS-T (0.25% Triton X-100) followed by blocking in PBS with antibody-specific serum (5%) or 1% BSA for 30 min. Primary antibodies (see Table S1 for details) were diluted in blocking solution and secondary antibodies were diluted 1,000-fold and incubated for 2 hr at room temperature in the dark. After washing, nuclei were stained with Hoechst 33258 (Sigma, H6024; 0.1 μg/mL in PBS) for 20 min and washed again with PBS. The ready stained plates were covered with aluminum foil and stored at 4°C in the dark until image acquisition. Imaging was performed on the confocal Opera HCS Reader (PerkinElmer), 20× objective, Laser lines (405, 488 nm). Laser power and excitation time was adjusted for each staining separately to avoid detector saturation and to allow signal detection in the linear range. The filter and camera settings were optimized using PerkinElmer filter selection tool to

avoid cross talk between channels. For each well, six images were taken at fixed positions for unbiased imaging. Images were stored for each Channel as flex files and finally imported in the Columbus-Data Base and Image analysis Software (PerkinElmer).

Yeast Strains and Growth Conditions

The *Saccharomyces cerevisiae* strains used in this study are derived from YPH499 (MATa, ade2-101, his3-Δ200, leu2-Δ1, ura3-52, trp1-Δ63, lys2-801). Mas1 mutant strains were generated by plasmid shuffling: YPH499 was transformed with a Yep352 plasmid encoding Mas1 under control of the MET25 promoter and CYC1 terminator. The chromosomal gene *MAS1* was disrupted using a *his3* cassette. The resulting strain was transformed with the pFL39 plasmid encoding Mas1 under its endogenous promoter and terminator region, in which the mutations had been introduced using site-directed mutagenesis. Cells were selected for plasmid loss by growth on medium supplemented with 5-fluoroorotic acid (5-FOA). The following strains were used for analysis: Mas1 (#4944; #5103), $Mas1^{Arg144Cys}$ (#4945), $Mas1^{Thr170Pro}$ (#4946), $Mas1^{Arg144His}$ (#5104) (these strains expressed Mas1 with an additional C-terminal HA tag), and Mas1 (#5101) and $Mas1^{Val146Gly}$ (#5102).

For growth tests, yeast strains were grown overnight in 5 mL YPG medium (1% (w/v) yeast extract, 2% (w/v) bacto peptone, 3% (w/v) glycerol [pH 5.0]) at 23°C. Cell numbers (OD_{600}) were measured and adjusted and serial dilutions spotted on YPD (2% (w/v) glucose instead of glycerol) and YPG agar plates. Plates were incubated at 23°C (− heat shock) and 37°C (+ heat shock).

Isolation of Mitochondria from Yeast and hPSC

Yeast strains were grown on non-fermentable medium at 23°C or shifted for 10 hr to 37°C prior to isolation of mitochondria. Cells were harvested in logarithmic growth phase (OD_{600} 0.8–1.0) and mitochondria were isolated by differential centrifugation.[36] Aliquots were snap-frozen in liquid nitrogen and stored in SEM buffer (250 mM sucrose, 1 mM EDTA, 10 mM MOPS-KOH [pH 7.2]) at −80°C. hPSC, NES, and HDF were washed with PBS and incubated in solution A (20 mM HEPES-KOH [pH 7.6], 220 mM mannitol, 70 mM sucrose, 1 mM EDTA, 0.5 mM PMSF, 2 mg/mL BSA) for 15 min on ice. Subsequently cells were homogenized by 30 strokes using a glass potter. Samples were centrifuged at 800 × *g* for 5 min at 4°C to remove unbroken cells and cellular debris. The supernatant was subjected to centrifugation at 7,000 × *g* for 15 min at 4°C. The obtained mitochondrial pellet was resuspended in solution B (solution A without BSA) and the protein concentration adjusted to 10 mg/mL with sucrose buffer (10 mM HEPES-KOH [pH 7.6], 0.5 M sucrose). Aliquots were stored at −80°C. Protein levels were analyzed by SDS-PAGE and western blotting according to standard protocols using the antibodies listed in Table S1.

In Organello Import of Radiolabeled Precursor Proteins

Radiolabeled precursor proteins were synthesized *in vitro* using the rabbit reticulocyte lysate system (Promega) in the presence of ^{35}S-methionine. Isolated yeast mitochondria (30 μg) and radiolabeled precursors were incubated in import buffer (10 mM MOPS-KOH [pH 7.2], 3% BSA, 250 mM sucrose, 5 mM $MgCl_2$, 80 mM KCl, 5 mM KP_i) supplemented with 2 mM ATP and NADH for the indicated time points at 23°C. Alternatively, mitochondria were subjected to an *in organello* heat shock (15 min 37°C) prior to addition of precursor, followed by import at 37°C. The membrane potential was disrupted by addition of AVO (8 μM antimycin A, 1 μM valinomycin, 20 μM oligomycin). Samples were treated with 50 μg/mL Proteinase K (Prot. K) for 10 min on ice to digest non-imported precursor proteins. Mitochondria were re-isolated by centrifugation at 16,000 × *g* for 10 min at 4°C and washed with SEM buffer. Samples were analyzed via SDS-PAGE and autoradiography.

In Vitro Processing

Isolated mitochondria (40 μg) were solubilized in reaction buffer (10 mM HEPES-KOH [pH 7.5], 1 mM $MnCl_2$, 1 mM DTT) containing 0.5% digitonin, incubated for 15 min on ice, and centrifuged at 10,000 × *g* for 10 min at 4°C. Obtained supernatant was incubated with radiolabeled frataxin (FXN) precursor for various time points at 37°C and analyzed by SDS-PAGE followed by western blotting and autoradiography.[37]

Blue-Native PAGE

Respiratory chain complexes were analyzed by Blue-native polyacrylamide gel electrophoresis. Mitochondria (50 μg) were solubilized in digitonin buffer (1% (w/v) digitonin, 20 mM Tris-HCl [pH 7.4], 0.5 mM EDTA, 10% (v/v) glycerol, 50 mM NaCl) and incubated on ice for 15 min. Samples were centrifuged at 20,000 × *g* for 5 min at 4°C and the supernatant was loaded on a 4%–13% gradient BN-PAGE followed by western blotting.

Membrane Potential Measurement

The membrane potential ($\Delta\psi$) of mitochondria was assessed by fluorescence quenching using the potential-sensitive fluorescent dye 3,3′-dipropylthiadicarbocyanine iodide. Isolated mitochondria (50 μg) were incubated in membrane potential buffer (0.6 M sorbitol, 0.1% (w/v) BSA, 10 mM $MgCl_2$, 0.5 mM EDTA, 20 mM KP_i [pH 7.2]). The membrane potential was dissipated by addition of valinomycin.[37]

Iron-Sulfur Cluster Biogenesis Desulfurase (ISD) Complex Formation

Labeling of the ISD complex using ^{35}S-cysteine was performed as described previously.[38] In brief, mitochondria (100 μg) were incubated in labeling buffer (0.6 M sorbitol, 20 mM Tris [pH 7.2], 0.15 mM KCl, 15 mM KH_2PO_4, 12.5 mM $MgCl_2$, 3 mg/mL BSA) supplemented with 0.875 mg/mL chloramphenicol for 15 min at 20°C. Mitochondria were isolated by centrifugation at 20,000 × *g* for 5 min at 4°C, solubilized in digitonin buffer (containing 0.4% digitonin) in the presence of 1 mM NADH, 2 mM ATP, and ^{35}S-methionine or ^{35}S-cysteine, and incubated for 15 min at 20°C. Samples were analyzed via BN-PAGE and autoradiography.

Human Tissue Biopsy Studies

Respiratory chain enzyme activities in muscle tissue were measured spectrophotometrically in post-600 g supernatants of individual A:II-1 and compared to a range determined from more than 20 control biopsies as described.[39] Blue native PAGE with in-gel activity staining for respiratory chain complexes I, II, IV, and V was performed on isolated membrane fractions obtained from tissues as described.[39,40] The assembly of respiratory chain complex I was analyzed in isolated mitochondrial membrane fractions from individual A:II-1 fibroblasts using BN-PAGE and by western blotting using an antibody against NDUFS2, a component of the earliest assembly intermediates.[41,42] Total aconitase activity in fibroblasts and muscle homogenates was measured spectrophotometrically.[43] The mitochondrial and

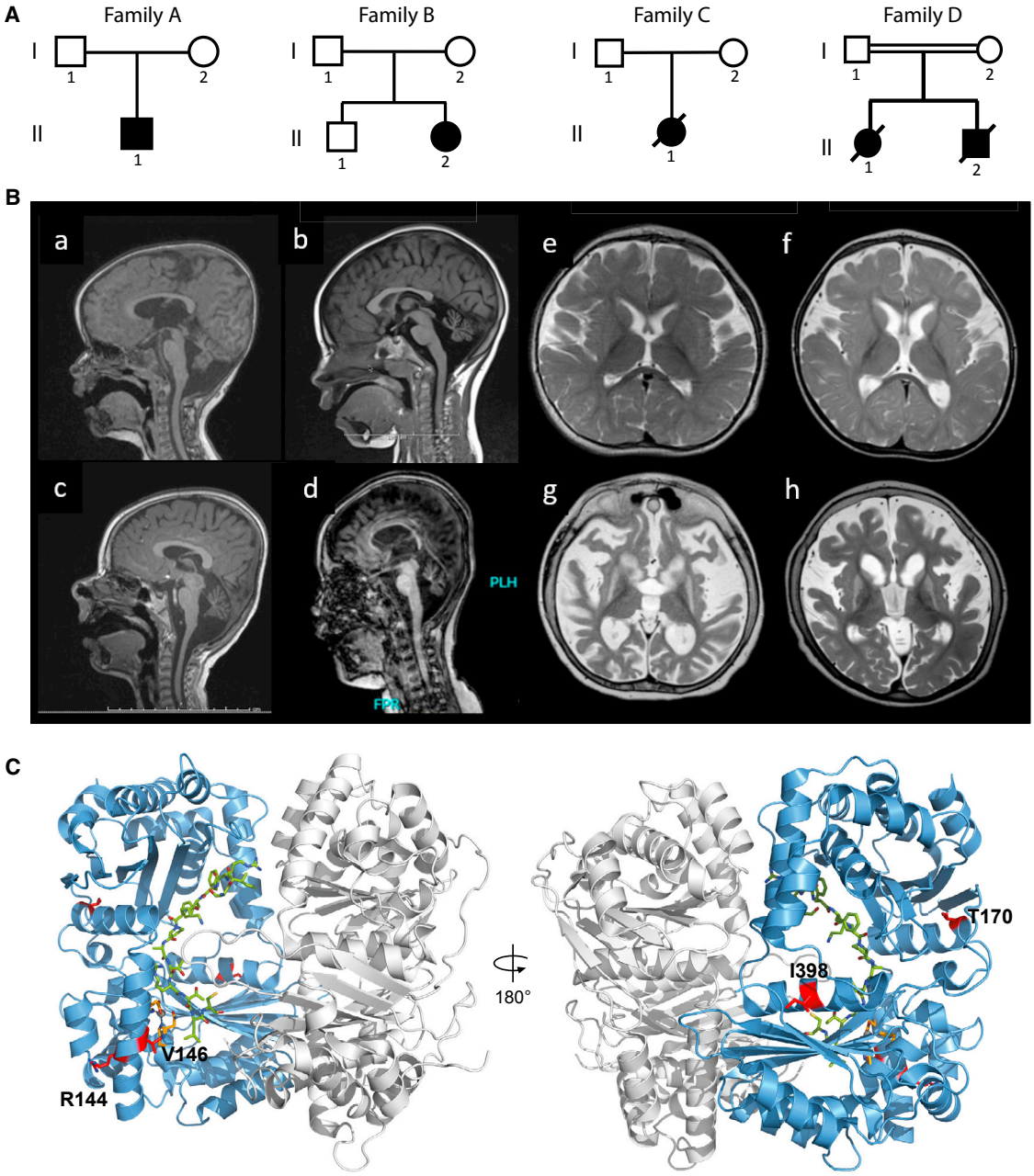

Figure 1. Genetics and MRI of Individuals Carrying *PMPCB* Variants
(A) Pedigrees of all families with *PMPCB* pathogenic variants. Black symbols designate affected individuals.
(B) Sagittal T1 MRI images of individual A:II-1 at 13 months (a), individual B:II-2 at 4 years (b), individual C:II-1 at 3 years (c), and individual D:II-1 at 3 years 3 months (d) demonstrating cerebellar atrophy in all four individuals. T2 transverse images of individual D:II-1 at 1 year (e) and 4 years 7 months (g) and individual D:II-2 at 9 months (f) and 3 years, 3 months (h), demonstrating progressive cerebral atrophy.
(C) Model of the crystal structure of the yeast MPP heterodimer (Mas1, blue; Mas2, gray) with the bound presequence peptide (green) in front (left) and back (right) view. The active site (yellow) and the positions of the mutations (red) are shown in stick representation.

cytoplasmic aconitase enzymes were separated on a gel and the activities measured individually using an in-gel activity stain as described.[44,45] The relative proportion of the activities from mitochondrial and cytosolic aconitase was distributed over the total activity as measured spectrophotometrically to provide the activity of each enzyme separately. The assay has a coefficient of variation of <7% for each fraction. Protein steady-state levels were assayed by SDS-PAGE and western blotting. Lipoylation of the E2 components of pyruvate dehydrogenase and α-ketoglutarate dehydrogenase was evaluated using an anti-lipoid acid antibody.[45] All antibodies used are listed in Table S1.

Results

Clinical Report

We identified five affected individuals from four unrelated families (Figure 1A). Clinical information for all individuals

is summarized below and in Table 1 and is presented in detail in the Supplemental Note. All affected individuals presented with significant developmental regression or stagnation within the first 2 years of life, which followed a minor illness or vaccination in three children. Common neurological features included truncal hypotonia, lack of independent ambulation, and lack of speech. Seizures were observed in four of the five children with onset between 11 months and 24 months, including generalized tonic-clonic seizures in the setting of fever, epileptic spasms, tonic seizures, and focal dyscognitive seizures. Features reported in a subset of affected individuals include ataxia, dystonia, acquired microcephaly, and spastic quadriplegia. Three affected individuals demonstrated clinical deterioration and early death before age 6 years. Brain MRI revealed T2 hyperintensities of the basal ganglia in all affected individuals (Figure 1B). Other observed brain MRI abnormalities included cerebral and cerebellar atrophy, which was demonstrated to be progressive in three individuals. Metabolic testing revealed elevated serum lactate in three, mild to borderline elevated serum pyruvate in two, and mildly elevated serum alanine in three of the five individuals.

Molecular Results and Structural Modeling

Molecular genetic testing of individual A:II-1 revealed a normal mtDNA sequence. Trio-based WES showed compound heterozygosity for two rare variants in *PMPCB* (GenBank: NM_004279.2): c.523C>T (p.Arg175Cys) and c.601G>C (p.Ala201Pro). Homozygous null mutations in *ACY1* were detected, which were considered a benign diagnosis and not consistent with the phenotype.

Trio-based WES of individual B:II-2 identified the same *PMPCB* variants as in individual A:II-1: c.523C>T (p.Arg175Cys) and c.601G>C (p.Ala201Pro). Individual B:II-2 also has a single variant in *PPT1* (GenBank: NM_000310.3; c.236A>G [p.Asp79Gly]), but no clinical or biochemical features of Batten's disease and assessment of PPT1 enzymatic activity revealed normal values (62 pmol/hr/spot, reference range 21–200 pmol/hr/spot).

WES in individual C:II-1 identified two rare variants in *PMPCB*, c.530T>G (p.Val177Gly) and c.524G>A (p.Arg175His), the latter affecting the same Arg175 as in individuals A:II-1 and B:II-2. Sanger sequencing in parents revealed that individual C:II-1 carried these mutations in a compound heterozygous state.

A diagnostic gene panel in individual D:II-1 for 72 epilepsy-related genes (CeGAT, Germany, Epi02 panel) did not reveal pathogenic variants. Trio exome sequencing identified a homozygous variant in *PMPCB* c.1265T>C (p.Ile422Thr) in individual D:II-1, which was subsequently confirmed in the affected brother (D:II-2) and both parents were heterozygous. A known SNP c.1188G>T (p.Glu396Asp) in *PMPCB* was also identified (rs3087615). Array comparative genomic hybridization (CGH) in individuals D:II-1 and D:II-2 was unremarkable.

As all four *PMPCB* variants identified in the affected individuals affect amino acid residues that are highly conserved (Figure S1), the crystal structure of yeast MPP[11] was used to assess potential effects of the mutations (Figures 1C and S2). The side chain of Arg144 is engaged in several hydrogen bonds that stabilize the protein fold, which the mutated residues (histidine and cysteine) cannot maintain (Figure S2A). Val146 is surface exposed and in proximity to the active site region (Figure S2B). Thr170 is located at the C-terminal end of an α helix and mutation to proline terminates the helix earlier (Figure S2C). Ile398 contributes to the packing of an α helix to a β sheet and lies close to the Mas1/Mas2 dimer interface. Mutation to a threonine results in a decreased side chain volume, hence altered packing and might impact on the heterodimer interaction (Figure S2D). Taken together, while the mutations do not directly affect the catalytic activity, they potentially result in changes of the stability of the protein's fold, accessibility of the active site, or dimer formation.

Generation and Characterization of Affected Individual-Derived hiPSCs and NES

We obtained dermal fibroblasts from individual D:II-2 bearing the homozygous c.1265T>C (p.Ile422Thr) variant in *PMPCB* and derived hiPSC lines thereof. Several colonies with hPSC-like morphology were manually picked and expanded to generate three independent iPSC lines (D:II-2.4, D:II-2.9, D:II-2.11) for further characterization. In parallel, control hESC (C1) and hiPSC lines (C2.2, C2.5) were obtained or generated from healthy individuals who had no variants in *PMPCB*. We confirmed pluripotency by immunocytochemical marker staining and PluriTest[32] analysis (Figures 2A, S3A, and S3B) in all hESC and hiPSC cell lines. All hiPSC cell lines were furthermore tested for karyotypic stability with G-banding (Figures S3C–S3E). In addition, to enable experimental analysis of cells that resemble the tissue predominantly affected in the *PMPCB* individuals, we differentiated both control and PMPCB hiPSCs toward neuroepithelial stem cells (NES).[33,35] Differentiation was confirmed by immunocytochemical staining (Figures S4A and S5).

Control and affected individual hiPSCs and NES cells were expanded and mitochondria isolated. The protein steady-state levels of PMPCB were analyzed by SDS-PAGE and western blotting and revealed a decrease in PMPCB levels in all three affected individual hiPSC and NES lines (Figures 2B, 2C, S4B, and S4C). Furthermore, PMPCB displayed a change in migration behavior in mitochondria isolated from cells derived from the affected individual as it shifted to a slightly higher molecular weight. Protein levels of PMPCA, which together with PMPCB forms the active MPP heterodimer, were only mildly affected. We analyzed additional mitochondrial proteins that are substrates of MPP (FXN, NDUFA9, GRP75, Rieske). While the protein levels of NDUFA9, GRP75, and Rieske were unchanged in control and affected individual mitochondria, analysis of frataxin (FXN) demonstrated a strong increase in its intermediate form and a reduction of the mature

Table 1. Biochemical and Clinical Findings in Individuals with *PMPCB* Variants

Individual	A:II-1	B:II-2	C:II-1	D:II-1[a]	D:II-2[a]
Sex	**M**	**F**	**F**	**F**	**M**
Genotype	c.523C>T (p.Arg175Cys), c.601G>C (p.Ala201Pro)	c.523C>T (p.Arg175Cys), c.601G>C (p.Ala201Pro)	c.524G>A (p.Arg175His), c.530T>G (p.Val177Gly)	c.1265T>C (p.Ile422Thr) homozygous	c.1265T>C (p.Ile422Thr) homozygous
Onset of symptoms	6 months	12 months	10 months	4 months	7 months
Current age/age of death	5 years	6 years 1 month	death at age 5 years and 6 months	death at age of 6	death at age of 5 years and 5 months
Developmental regression	12 months	12 months	no distinct period of regression	12 months	8 months
Unable to ambulate	+	+	+	+	+
Lack of speech	+	+	+	+	+
Seizures/epilepsy	+	+	−	+	+
MRI brain findings	progressive cerebellar atrophy and signal abnormality, basal ganglia signal abnormalities	cerebellar atrophy, basal ganglia signal abnormalities	cerebellar and brain stem atrophy, abnormal signal of basal ganglia and cerebral white matter	progressive diffuse atrophy, basal ganglia signal abnormalities	progressive diffuse atrophy, basal ganglia signal abnormalities
Elevated serum lactate	+	+	+	−	−
Other clinical findings	severe ataxia and dystonia; poor weight gain		optic atrophy, severe dystonia; poor weight gain	refractory epileptic encephalopathy	refractory epileptic encephalopathy
Mitochondrial enzyme studies of skeletal muscle	decreased activity of respiratory chain complexes; decreased cytosolic and mitochondrial aconitase activity	ND	ND	decreased complex IV and citrate synthase activity	ND
Biochemical analysis of fibroblast mitochondria	increased iFXN, decreased mFXN and PMPCB level; accumulation of respiratory complex I subcomplexes	ND	ND	ND	increased iFXN, decreased mFXN and PMPCB level
Analysis of homologous Mas1 yeast mutants	lethal growth defect upon heat shock; severe MPP processing defect and early defect in Fe-S-cluster biogenesis at elevated temperature	lethal growth defect upon heat shock; severe MPP processing defect and early defect in Fe-S-cluster biogenesis at elevated temperature	lethal growth defect upon heat shock; severe MPP processing defect and early defect in Fe-S-cluster biogenesis at elevated temperature	lethal	lethal
iPSC/NES analysis	ND	ND	ND	ND	increased iFXN, decreased mFXN and PMPCB level; enhanced formation of ISD complex

ND, not determined.
[a]siblings

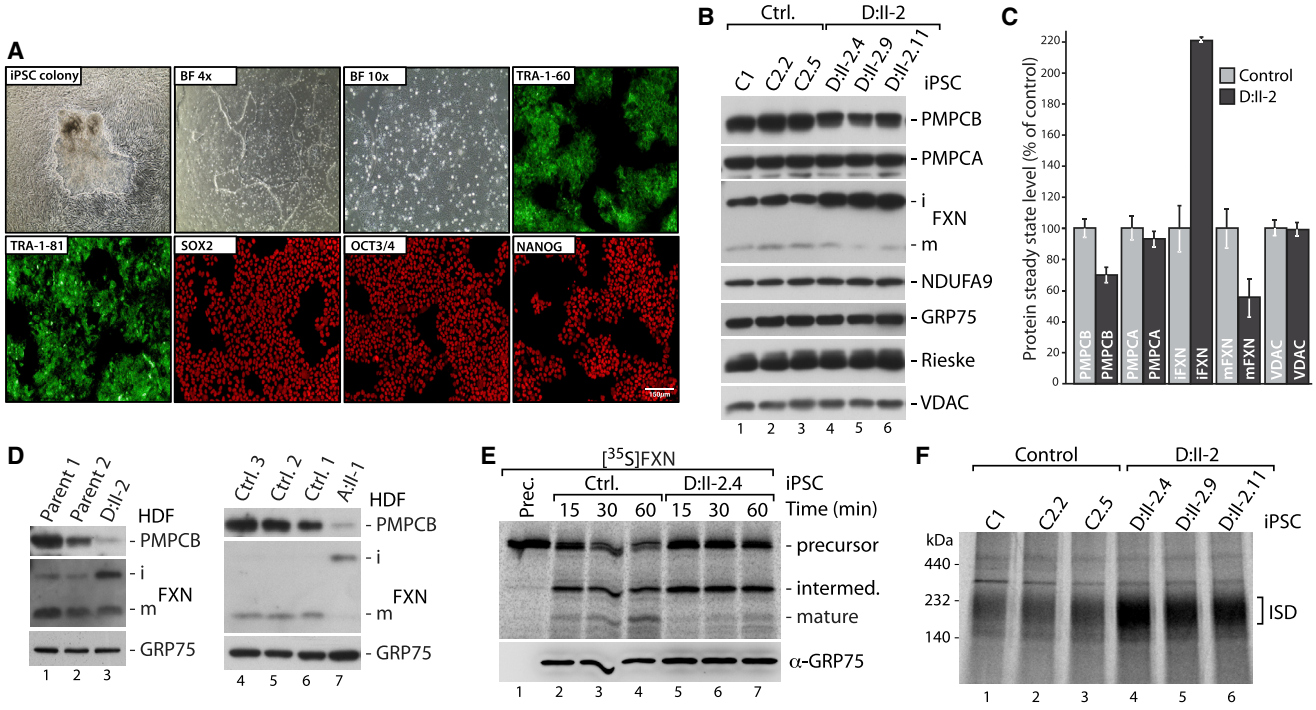

Figure 2. Analysis of Mitochondria Isolated from *PMPCB* iPSCs and Dermal Fibroblasts

(A) Morphology and ICC-based characterization of hiPSC clone D:II-2.11 derived from affected individual D:II-2. BF, bright field.

(B) Protein steady-state levels of mitochondria isolated from three different *PMPCB* iPSC cell clones (D:II-2.4, D:II-2.9, D:II-2.11) and controls (Ctrl.). i, intermediate; m, mature.

(C) Quantifications of protein steady-state levels from (B). Values represent mean ± SEM (error bars; n = 3).

(D) Protein steady-state analysis of mitochondria isolated from fibroblasts of family D with affected individual D:II-2 and individual A:II-1 and controls (Ctrl. 1–3).

(E) Processing of radiolabeled Frataxin (FXN) precursor in mitochondrial extract from affected individual D:II-2 (D:II-2.4) and control (Ctrl., C2.2) iPSC line. α-GRP75, loading control.

(F) Formation of ISD complex in mitochondria isolated from control (C1, C2.2, C2.5) and affected individual (D:II-2.4, D:II-2.9, D:II-2.11) hiPSC lines.

protein. As fibroblasts represent the main resource material obtainable from affected individuals, we next assessed PMPCB and FXN levels in mitochondria isolated from primary dermal fibroblasts. Interestingly, the same aberrant FXN processing and decreased PMPCB levels were observed in fibroblast mitochondria of individuals D:II-2 and A:II-1 (Figure 2D). The FXN precursor is processed twice by MPP, generating an intermediate and mature protein.[46,47] The accumulation of intermediate frataxin (iFXN) pointed toward a decrease in MPP activity in the PMPCB mutant. We therefore aimed to assess MPP enzymatic activity directly by generating mitochondrial extract from control and PMPCB mutant mitochondria and incubation with radiolabeled FXN precursor protein (Figure 2E).[37] MPP processed FXN efficiently to its intermediate and mature form in the control mitochondria. PMPCB mutant mitochondria also demonstrated efficient precursor processing; however, iFXN accumulated and processing to the mature form was severely hampered. Therefore, the homozygous c.1265T>C (p.Ile422Thr) *PMPCB* variant results in an incomplete maturation of the FXN protein *in vivo* and *in vitro*.

The observation of an *in vivo* MPP processing defect only for frataxin was surprising as the accumulation of iFXN and the lower amount of mature FXN pointed toward a strong decrease in MPP activity in the affected individual samples. FXN is involved in the biogenesis of Fe-S clusters in the mitochondrial matrix. This biosynthetic pathway is essential as critical cellular mechanisms such as nuclear DNA repair enzymes are dependent on Fe-S clusters.[48–50] iFXN plays a physiological role in Fe-S-cluster biogenesis as it can transfer Fe^{2+} and Fe^{3+} to the ISCU/NFS1/ISD11 iron-sulfur assembly complex.[51,52] In comparison to iFXN, mature FXN binds iron more labile and does not interact as strongly with the ISCU/NFS1/ISD11 complex. It has therefore been proposed that an increase in iFXN protein level provides a mechanism for the cell to increase the rate of Fe-S-cluster biogenesis in times of higher demands such as during cell growth or mitochondrial biogenesis. Mature frataxin (mFXN) is predominant under steady-state conditions in non-dividing cells as it has a lower Fe-S-cluster biogenesis rate.[51]

hPSCs are usually cultured in high-glucose medium and do not use mitochondria for oxidative phosphorylation.[30,53] However, the role of mitochondria in the biosynthesis of Fe-S clusters remains essential in hPSCs even in the absence of respiration. We examined how the increased iFXN affected Fe-S-cluster biogenesis by

analyzing the capacity of acquiring sulfur in hPSC and NES lines. The ISD complex represents an intermediate assembly during Fe-S-cluster biogenesis formed by NFS1 and ISD11 that detach sulfur from cysteine and transfer it to the ISCU protein.[38] FXN is an allosteric activator of this step. Formation of the ISD complex was strongly increased in hPSC and NES mitochondria of the affected individual D:II-2 with the homozygous c.1265T>C (p.Ile422Thr) *PMPCB* variant (Figures 2F, S4D, and S4E). Together with the increased iFXN level, this indicates an enhanced Fe-S-cluster biogenesis in the PMPCB mutant mitochondria from hPSCs.

Given the limitations of studying mitochondrial respiratory chain function in hPSCs due to their glycolytic metabolism and mitochondrial immaturity, we wanted to assess the effect of mutated PMPCB in a model organism that would allow for a switch between glycolytic and respiratory cell growth upon increased mitochondrial biogenesis and full functional activity.

PMPCB Mutations Impair Presequence Processing by MPP

The human PMPCB and the yeast homologous Mas1 are highly conserved and all *PMPCB* variants result in amino acid changes at conserved positions (Figure S1). Therefore, we used the yeast *Saccharomyces cerevisiae*, in which mitochondrial protein biogenesis has been analyzed in detail, to model the identified *PMPCB* mutations. The yeast model enabled us to analyze the function of MPP under various metabolic (fermentable versus respiratory) and stress conditions (e.g., heat stress). Mas1 is encoded by an essential gene[54] and its deletion is lethal under any growth condition. We therefore introduced the homologous mutations of affected individuals A:II-1 and B:II-2 ($Mas1^{Arg144Cys}$, $Mas1^{Thr170Pro}$) and individual C:II-1 ($Mas1^{Arg144His}$, $Mas1^{Val177Gly}$) by the plasmid shuffling approach. Introduction of the mutation identified in individuals D:II-1 and D:II-2 ($Mas1^{Ile398Thr}$) did not yield viable yeast strains. We first assessed cell growth under fermentable and respiratory conditions at different temperatures. All Mas1 mutant yeast strains grew comparable to wild-type yeast at standard growth temperatures (e.g., 23°C). However, inducing cellular stress by heat shock at 37°C led to a severe impairment of cell viability (Figures 3A and S6A). Notably, this impaired cell growth is observed under respiratory (glycerol as carbon source) but also fermentative (glucose as carbon source) conditions indicating that the mutations affect essential mitochondrial functions.

To explore whether impaired cell growth upon heat shock is due to loss of enzymatic MPP activity in the mutant Mas1 cells, MPP function was directly assessed by *in organello* import experiments of radiolabeled precursor proteins into mitochondria isolated from cells grown at 23°C. When the import experiments were performed at low temperature, MPP processing activity was comparable in wild-type and mutant Mas1 mitochondria (Figure S6B and S6C). However, following a 15 min *in organello* heat shock prior to the import reaction (Figures 3B and S6D), a severe decrease in MPP processing activity in the mutant mitochondria was noted reflected in the accumulation of non-processed precursor proteins (Atp2, Sod2, Mdh1) inside mitochondria. Overall import competence was not affected as demonstrated by import of Hsp10, which uses the same protein import pathways but is not cleaved by MPP (Figure 3B).[37] Therefore, presequence processing activity of mutant MPP is severely hampered under heat stress.

As MPP is the major presequence processing protease in mitochondria, we assessed the consequences of MPP inactivation *in vivo* by applying a heat shock to yeast cell cultures prior to isolation of mitochondria and testing an array of proteins which are imported via the presequence import pathway by immunoblotting (Figures 3C and S6E).[6,8,55] Reflecting a severely impaired MPP function, compared to wild-type mitochondria, every presequence-targeted protein tested showed a significant accumulation of the immature precursor, and many also showed a decreased level of the fully processed, mature form. The affected proteins carry out various mitochondrial functions including reactive oxygen detoxification (Sod2), protein biogenesis and folding (Mdj1, Mge1, Hsp60), oxidative phosphorylation (Cox4, Cox6, Rip1, Atp2, Atp3), the citric acid cycle (Mdh1), and Fe-S-cluster biogenesis (Jac1). The mutations in Mas1 when challenged at 37°C affect processing of all incoming precursor proteins that possess presequences. Also, the Mas1 protein accumulated immature species, as it is processed by MPP upon import. Mutant Mas1 furthermore showed the same aberrant migration behavior as the homologous PMPCB mutant for p.Ile422Thr (compare western blot analysis of Mas1 in Figures 3C and S6E with PMPCB in Figures 2B and S4B). Control proteins, which are not substrates of MPP, were not affected and showed similar levels in wild-type and mutant mitochondria (Figures 3C, right panel and S6E, Msp1).

Taken together, the homologous mutations of the affected individuals A:II-1, B:II-2, and C:II-1 introduce a temperature-sensitive phenotype in the yeast Mas1 protein that leads to a loss of MPP function upon *in organello* or *in vivo* heat stress.

Mas1 Mutations Impact on the Essential Biogenesis of Fe-S Clusters

We hypothesized that yeast grown at permissive temperature (23°C) or exposed to heat stress could be an ideal tool to investigate the impact of the affected individuals' mutations on mitochondrial function. We speculated that yeast growth at 23°C may mimic cells from the affected individuals under resting steady-state conditions. Growth during heat stress may represent a model for cells of these individuals upon enhanced mitochondrial biogenesis, increased requirements of mitochondrial functions during growth and development, or cellular stress in the setting of fever or infection.

Most components of the respiratory chain complexes are imported via the presequence import pathway and

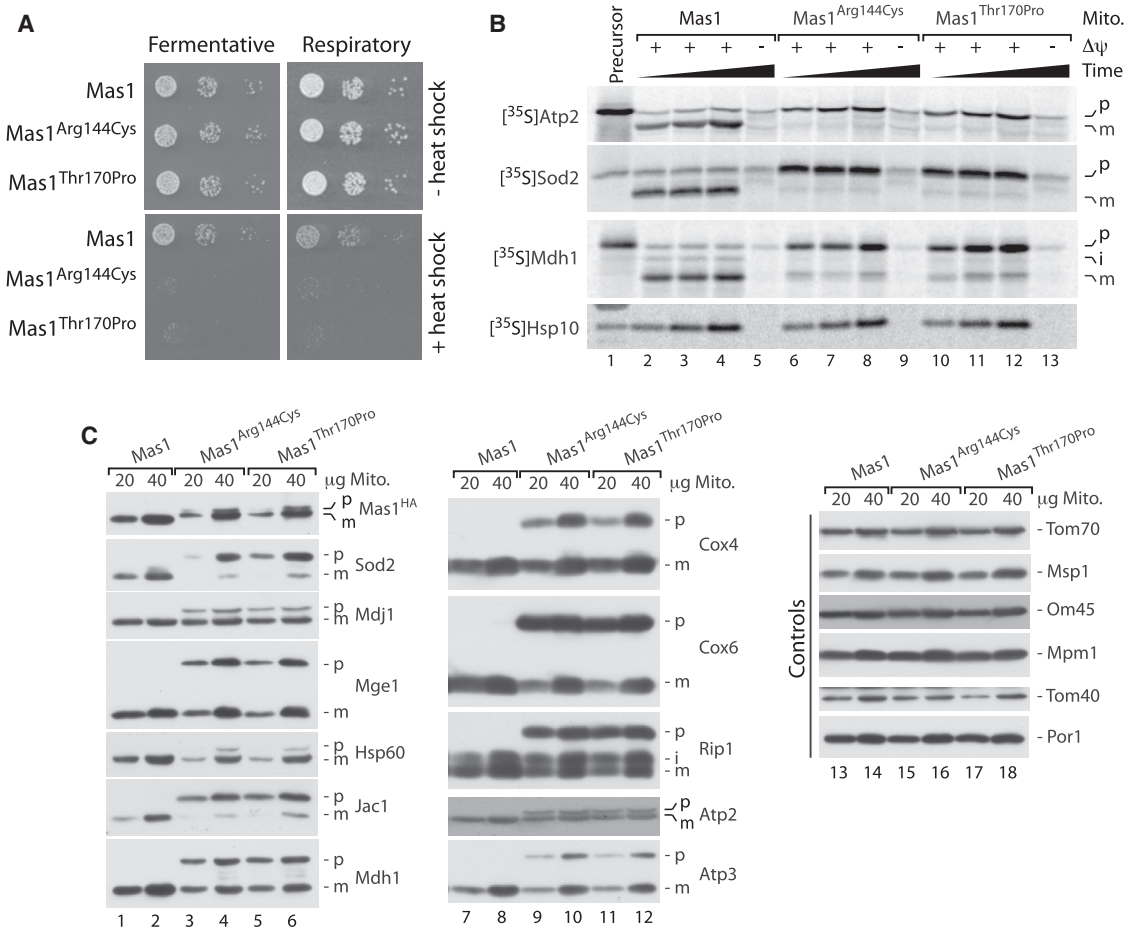

Figure 3. Analysis of *PMPCB* Mutations in Yeast
(A) Growth of Mas1 wild-type, Mas1^{Arg144Cys}, and Mas1^{Thr170Pro} mutant yeast strains under fermentative and respiratory conditions.
(B) Import of radiolabelled precursors upon *in organello* heat shock into mitochondria isolated from wild-type and Mas1 mutant cells. p, precursor; i, intermediate; m, mature.
(C) Western blot analysis of steady-state protein levels in Mas1 wild-type, Mas1^{Arg144Cys}, and Mas1^{Thr170Pro} mutant mitochondria isolated after *in vivo* heat shock.

consequently have to undergo presequence processing by MPP.[8,55,56] We analyzed the integrity of the respiratory chain complexes in mitochondria isolated from cells after growth at permissive temperature or after heat shock to impair MPP activity using blue native PAGE which resolves the native, intact complexes after solubilization with mild non-ionic detergents.[57] In yeast, complexes III and IV form supercomplexes containing two units of complex III and one or two units of complex IV.[58] Immunoblotting revealed no changes in respiratory chain complexes in mitochondria isolated after growth at permissive temperature (Figures 4A and S7A). Upon heat shock, a mild reduction of both supercomplexes (III_2IV_2 and III_2IV) in the mutant mitochondria was detected (Figures 4B and S7B). The same was observed for complex II, while the ATP synthase (dimer and monomer of complex V) was not affected (Figures 4B and S7B). Next, we measured the membrane potential Δψ across the inner membrane, which depends on highly functional mitochondria and can therefore be used as a marker for the fitness of these organelles. Three of the four Mas1 mutations led to a slight but significant reduction of Δψ when mitochondria were isolated after growth at elevated temperature (Figures 4C and S7C).

The biogenesis of Fe-S clusters represents the only essential mitochondrial function, making these organelles indispensable for life under any growth condition. Since frataxin, which showed processing defects in affected individual hPSCs and fibroblasts, is involved in iron-sulfur cluster biogenesis, we assessed the formation of the ISD complex (Figure S7D). While the complex was formed in the Mas1 mutants comparably to wild-type upon growth at permissive temperature, complex formation was severely reduced upon inactivation of MPP by exposing the cell cultures to heat stress (Figures 4D and S7E). Thus early steps in the iron-sulfur cluster biosynthesis are clearly impaired.

Affected Individual Tissues Show Dysfunction of Iron-Sulfur Cluster Containing Enzymes

To study the functional impact of the PMPCB mutations in the affected individuals, several cellular functions

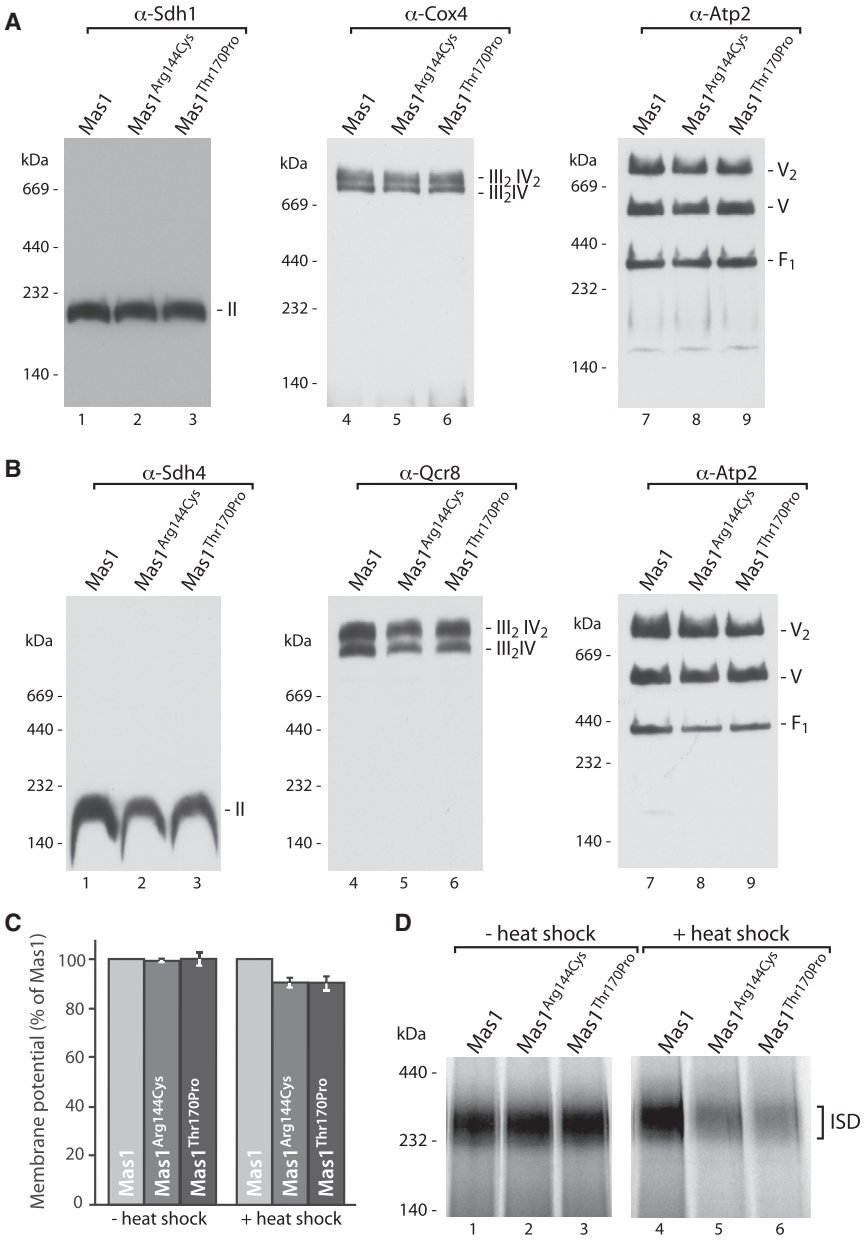

Figure 4. Characterization of Mitochondrial Functions in Mas1 Mutant Yeast Cells
(A) BN-PAGE analysis of respiratory chain complexes in Mas1 wild-type and mutant mitochondria isolated after cell growth at 23°C.
(B) Analysis as in (A), mitochondria were isolated after *in vivo* heat shock.
(C) Membrane potential measurement in mitochondria isolated from Mas1, $Mas1^{Arg144Cys}$, and $Mas1^{Thr170Pro}$ cells after growth at permissive temperature (– heat shock; values represent mean ± SEM, n = 4) or *in vivo* heat shock (+ heat shock; values represent mean ± SEM, n = 3).
(D) ISD complex formation in Mas1 wild-type and mutant mitochondria isolated at 23°C (– heat shock) or after *in vivo* heat shock.

were reviewed in tissues from individual A:II-1. While enzyme activities of the respiratory chain were normal in fibroblasts and liver, complex II activity was significantly reduced in muscle (Table 2). Analysis of respiratory chain complexes using blue native PAGE with in-gel activity staining confirmed the severely decreased complex II activity in the A:II-1 muscle biopsy (Figure 5A) and protein steady-state analysis on SDS-PAGE also revealed mildly reduced levels of respiratory chain subunits (Figure S8A). Furthermore, blue native PAGE analysis of mitochondrial membrane fractions from A:II-1 fibroblasts followed by western blotting identified accumulation of several subassemblies of complex I at 100, 230, 400, 460, and 830 kDa, whereas in the assay control and all previously analyzed ten control fibroblasts only the fully assembled holocomplex at 1 MDa and a small amount at 230 kDa were visible (Figure 5B).[41] This shows an impact on complex I assembly, even though the amount of holocomplex was comparable to control mitochondria such that enzyme function was preserved.

As the respiratory chain complexes I, II, and III contain several iron-sulfur clusters, and Mas1 mutations severely decreased cluster biogenesis, other Fe-S-cluster-dependent enzymes such as lipoic acid synthetase (LIAS) involved in lipoylation of mitochondrial proteins and aconitase were evaluated. The protein steady-state levels of lipoylated E2 subunits of pyruvate dehydrogenase and α-ketoglutarate dehydrogenase were normal in fibroblasts and muscle of individual A:II-1 revealing normal functional activity of LIAS (Figure S8B). While the mitochondrial and cytosolic aconitase activity of affected individual fibroblasts was comparable to control (Figure 5C), the enzymatic activity of both enzymes was deficient in muscle tissue of individual A:II-1 (Figure 5D), even though the protein levels of both aconitase enzymes remained normal (Figure S8C), likely because the defect affected the Fe-S cofactor rather than the apoenzyme. Thus, several iron-sulfur cluster containing mitochondrial and cytosolic enzymes are affected and this defect is more pronounced in muscle tissue than in fibroblasts. In all tissues analyzed, normal amounts of mature citrate synthase, which has an MPP cleavable leader sequence, were detected (Figure S8C), illustrating that in this relatively less severely affected individual, the impact on cellular bioenergetics is not a generalizable effect on protein processing but specific to iron-sulfur cluster biogenesis.

Table 2. Enzyme Activities of Respiratory Chain Complexes and Citrate Synthase Normalized to Total Protein Content of Control and Affected Individual A:II-1 Muscle Tissue

	Activity[a] (Reference Range)	SD[b]	% of Control Mean	Activity/Citrate Synthase[a] (Reference Range)	SD[b]
Complex I	23.5 (23.6–74.8)	−1.7	52%	120 (98–271)	−1.5
Complex II	25.8 (49.0–133.4)	−3.5	29%	131 (251–573)	−3.6
Complex III	11.6 (5.7–31.4)	−0.3	67%	59 (19–172)	−0.1
Complex II + III	30.7 (34.2–107.6)	−1.7	49%	157 (173–472)	−1.8
Complex IV	1.2 (1.1–3.8)	−1.7	45%	6 (4–23)	−1.7
Citrate synthase	196.1 (159.8–353.3)	−0.9	76%	NA	NA

[a]The activity in nmol·min^{-1}·protein^{-1} and the ratio of the activity over citrate synthase is shown.
[b]The distribution of the results from controls (n = 25) when log transformed is normal, and the affected individual value expressed as a Z-score of this control range. A SD of < -2 is considered significant. NA, not applicable.

Discussion

In this study, we identify four families with biallelic pathogenic variants in *PMPCB*, encoding the catalytic subunit of MPP. The phenotypic features in all affected individuals include a combination of Leigh-like features of episodic regression and basal ganglia lesions, often in the setting of febrile illnesses, but also with prominent cerebellar atrophy and increased T2 signal of the cerebellar cortex (families A and B). The more severely affected individuals also had therapy-resistant epileptic encephalopathy (family D) or leukodystrophy (family C). The phenotype is similar to that reported in individuals with mutations in the non-catalytic MPP subunit *PMPCA* (MIM: 613036) of cerebellar ataxia[59,60] and early-onset mitochondrial encephalopathy.[61] The disorders secondary to mutations in *PMPCA* and *PMPCB* can jointly be considered disorders of MPP function. However, most of the reported *PMPCA* individuals have achieved independent ambulation and verbal language, which is a milder manifestation compared to the *PMPCB* phenotype. In the *PMPCA* individuals, the severity of disease seemed to depend on the mutation's vicinity to the glycine-rich loop of PMPCA, which has been implicated in substrate recognition and binding.[13] The more severe phenotype seen in the *PMPCB* individuals may be due to a stronger impact on MPP activity by mutations in the catalytic PMPCB subunit, suggesting a correlation of the variability of the phenotype and the degree of MPP dysfunction. First, while the Mas1 yeast cells bearing the homologous mutations of individuals A:II-1, B:II-2, and C:II-1 were viable at lower temperature, introduction of the *PMPCB* c.1265T>C (p.Ile422Thr) mutation of individuals D:II-1 and D:II-2 into yeast resulted in a lethal phenotype even at low temperature. Thus, a correlation exists between the phenotypic severity, the amount of steady-state PMPCB and Mas1 protein levels, and the impact of homologous mutations in Mas1 on the yeast growth phenotype, with mutation p.Ile422Thr representing a more severe phenotype than the other affected individuals' mutations, who share mutations affecting Arg175. Given the crucial role of MPP in processing 70% of all mitochondrial precursor proteins, dysfunction of MPP was long considered to be incompatible with life as it profoundly interferes with mitochondrial homeostasis.

Second, while the yeast model revealed the viable mutant Mas1 to be functional upon growth at lower temperature, heat stress triggered a lethal phenotype. This could be due to decreased stability or misfolding of mutant Mas1 resulting in the observed functional inactivation of MPP, or due to a mismatch between the mutant MPP processing ability and increased functional requirements upon enhanced mitochondrial protein biogenesis, and can relate to the regression with febrile illnesses observed in the affected individuals.

Third, cells that are mostly fermentative and have low mitochondrial demands such as stem cells or fibroblasts are less affected than primarily aerobic muscle tissue or neurons. It is tempting to speculate that under resting conditions PMPCB mutations can still maintain the basic functional requirements of mitochondria, which is also reflected in the hPSC/NES *PMPCB* lines. However, upon increased need for mitochondrial biogenesis during early childhood growth and development, or upon cellular stress in the setting of infection or fever, mitochondria with mutated PMPCB are insufficiently capable of adjusting to the increasing demands on precursor processing, hampering mitochondrial biogenesis, and resulting in neurological injury.

In vivo and *in vitro* analysis of PMPCB hPSCs, NES, and fibroblast mitochondria revealed a strong accumulation of iFXN and a block of its second MPP processing step. FXN is an unusual substrate as it undergoes two-step processing by MPP[46,47] and this sequential processing might render FXN especially sensitive toward MPP dysfunction. We hypothesize that the sequential processing of FXN might serve as a safety loop to ensure maintenance of Fe-S-cluster biosynthesis under stressed conditions or upon increased mitochondrial biogenesis in which an elevated protein import rate saturates the processing capacity of MPP. The two-step processing of FXN would then enable adaptation of FXN activity and thereby Fe-S-cluster biogenesis upon changes in cellular conditions.[51] The second

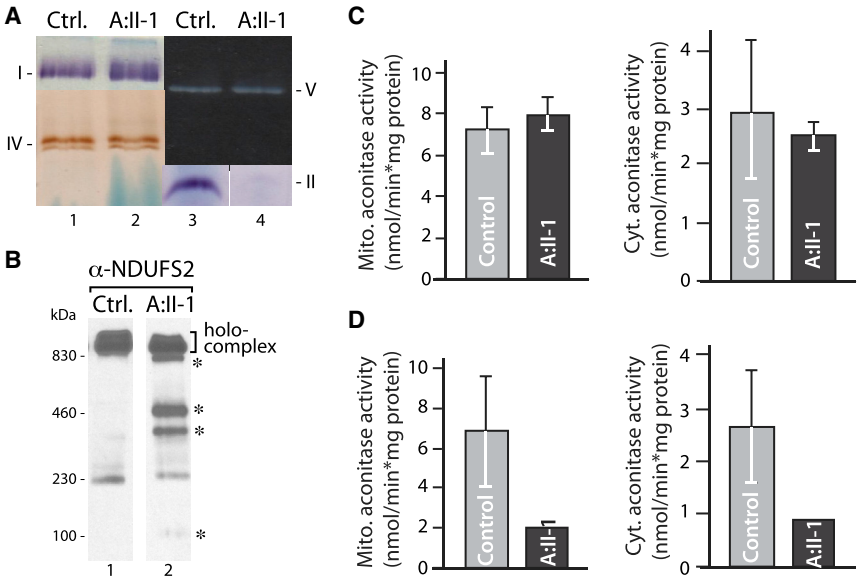

Figure 5. Analysis of Enzymatic Activity of Fe-S-Cluster-Containing Proteins and Protein Complexes in *PMPCB* Tissues

(A) Isolated mitochondrial membrane fractions of individual A:II-1 and control (Ctrl.) muscle samples were analyzed by BN-PAGE followed by in-gel activity staining for respiratory chain complex I, II, IV, and V.

(B) Assembly of respiratory chain complex I by BN-PAGE analysis in isolated mitochondrial membrane fractions obtained from affected individual A:II-1 and control fibroblasts. holocomplex, fully assembled complex I; *, lower molecular weight subcomplexes.

(C) Enzymatic activity of mitochondrial and cytosolic aconitase in fibroblasts of individual A:II-1 and control. Values represent mean ± SD (error bars; control n = 9, A:II-1 n = 5).

(D) Mitochondrial and cytosolic aconitase activity in muscle homogenates from individual A:II-1 and controls. Data are represented as mean ± SD (error bars; control n = 11, A:II-1 average of two measurements).

FXN processing has also been described as less efficient than the generation of FXN intermediates.[46] This might explain why only decreased mFXN protein levels have been detected in samples obtained of the affected individuals, while processing defects in other (one-step) MPP substrates were not yet observed.

The FXN protein itself has been studied extensively as loss of function causes the autosomal-recessive degenerative disease Friedreich ataxia (FRDA).[62,63] However, FRDA samples revealed a depletion of all FXN isoforms.[51,64] In contrast, mutations in *PMPCB* showed only a decrease in mFXN protein levels, while iFXN was even increased.

Our results suggest that biogenesis of Fe-S clusters is affected early upon MPP dysfunction and may represent the primary pathophysiologic mechanism triggered by mutations in the catalytic MPP subunit and its sensitive impact on FXN processing. Similar to mutations in iron-sulfur-cluster biogenesis defects, such as NFU1, BOLA3, NFS1, IBA57, or ISCU,[65–71] mutations in *PMPCB* impact the function of several iron-sulfur-cluster-containing enzymes particularly in muscle, the most affected tissue included in our analysis. Respiratory chain complex II is sensitive to iron-sulfur cluster dysfunction[65–71] and its enzymatic activity was virtually absent in the affected individual muscle biopsy. Assembly of complex I, which contains eight iron-sulfur clusters,[72] was hampered in fibroblast mitochondria leading to the accumulation of abnormal subcomplexes. In contrast to genetic defects in enzymes directly involved in Fe-S-cluster biogenesis,[65–71] but similar to frataxin deficiency,[73] there was normal lipoylation and activity of mitochondrial lipoate-bearing enzymes, indicating that lipoic acid synthetase (LIAS) activity, which depends on an Fe-S cluster, was still sufficiently preserved, likely explaining why the phenotype is less severe than seen in iron-sulfur-cluster biogenesis disorders such as *NFU1*. The enzymatic activity of both mitochondrial and cytosolic aconitase was severely decreased in muscle tissue. Aconitase activity was still preserved in cultured fibroblasts, which is a more glycolytic cell type than muscle and might therefore be less affected by the PMPCB mutations. After their synthesis in mitochondria, Fe-S clusters are exported from the organelle as they are essential for the enzymatic function of several nuclear and cytosolic proteins, including a pivotal role in DNA synthesis and repair, chromosome segregation, or protein translation processes. The decrease of the cytosolic aconitase activity indicates that the defects in Fe-S-cluster biogenesis triggered by mutations in PMPCB can affect mitochondrial bioenergetics and in addition cellular functions outside of the mitochondrial organelle, which also explains the growth defects of Mas1 mutant yeast under fermentative conditions.

The data on Fe-S-cluster biosynthesis in our *PMPCB* hPSC and NES lines differed from the results obtained in affected individuals' tissues, fibroblasts, and yeast. While Fe-S-cluster biosynthesis is an essential pathway in hPSC and NES lines, these models may have limitations when assessing the impact of PMPCB impairment on Fe-S-cluster biosynthesis under oxidative growth or stress conditions. While the increased iFXN levels and enhanced ISD complex formation suggested an elevation of Fe-S-cluster biogenesis in hPSC and NES PMPCB mitochondria, this biosynthesis pathway was decreasing early upon MPP inactivation in yeast mitochondria bearing the homologous Mas1 mutations. However, it is tempting to hypothesize that the increased ISD complex formation in hPSCs and NES is caused by the increased iFXN levels providing the cell with a mechanism to adapt Fe-S-cluster biogenesis to changes in cellular demands. Furthermore, our hPSC data and also analysis of the *PMPCA* individuals identified frataxin as an early marker for MPP dysfunction as it is the only MPP substrate identified to be affected in the *PMPCB* individuals *in vivo*.

Employing our yeast model, we could show that MPP dysfunction caused by the Mas1 mutations affects all presequence-possessing precursors. Therefore, we hypothesize that all mitochondrial functions will be ultimately affected by the mutations in *PMPCB* if conditions are severe enough and that the FXN levels and the data obtained in yeast point toward an early impact on Fe-S-cluster biogenesis. The stringent *in vivo* conditions that allow precise induction of MPP dysfunction in yeast underline the importance of unicellular model organism like *S. cerevisiae* to mimic and decipher pathogenic mechanisms that result in complex human diseases.

In summary, we identify *PMPCB* mutations in a mitochondrial disease resulting in Leigh-like neurodegeneration in childhood with prominent cerebellar atrophy. With the identification of biallelic pathogenic variants in *PMPCB*, we establish dysfunction of the catalytic subunit of the mitochondrial presequence processing protease as the disease mechanism accompanied by changes in iron-sulfur-cluster biogenesis.

Supplemental Data

Supplemental Data include Supplemental Note, eight figures, and one table and can be found with this article online at https://doi.org/10.1016/j.ajhg.2018.02.014.

Acknowledgments

We would like to thank all affected individuals and their family members for their participation in this study. Furthermore, we would like to thank Dr. Almuth Caliebe for her clinical care of one of the affected families. We thank Dr. Chris Meisinger for discussion, Dr. Elizabeth Craig for Jac1 antiserum, and Corina Mitchell and Jon Roberts for pathology work. The current study has been supported by the EuroEPINOMICS-Rare Epilepsy Syndrome (RES) consortium which provided capacity for exome sequencing. This work was supported by intramural funds of the University of Kiel (I.H.), the German Research Foundation (HE5415/3-1 to I.H.) within the EuroEPINOMICS framework of the European Science Foundation, the German Research Foundation (DFG, HE5415/5-1, HE5415/6-1 to I.H.), the BMBF (13GW0128A and 01GM1513D) (to B.B. and F.-J.M.), the Deutsche Forschungsgemeinschaft (DFG, MU3231/3-1 to F.-J.M.), the Excellence Initiative of the German Federal & State Governments Schleswig-Holstein Cluster of Excellence (EXC 306 Inflammation at Interfaces), the Emmy Noether-Programm of the Deutsche Forschungsgemeinschaft (to F.-N.V.), a grant for Research on Measures for Rare/Intractable Diseases from the Japan Agency for Medical Research and Development (to N. Matsumoto), and Grants-in-Aid for Scientific Research (A and B) from the Japan Society for the Promotion of Science (to N. Miyake and N. Matsuomto). This work also received financial support from Miracles for Mito, Summits for Samantha, and the Children's Hospital Colorado Foundation (J.L.K.V.H., A.L., and M.W.F.). Work included in this study has also been performed in partial fulfillment of the requirements for the doctoral thesis of C.K. In addition, D.N.S. is a full-time employee of Ambry Genetics. Exome sequencing is one of Ambry's commercially available tests.

Received: October 12, 2017
Accepted: February 19, 2018
Published: March 22, 2018

Web Resources

Addgene, http://www.addgene.org/
ClinVar, https://www.ncbi.nlm.nih.gov/clinvar/
dbSNP, https://www.ncbi.nlm.nih.gov/projects/SNP/
ExAC Browser, http://exac.broadinstitute.org/
GeneMatcher, https://genematcher.org/
OMIM, http://www.omim.org/
UCSC Genome Browser, http://genome.ucsc.edu
wANNOVAR, http://wannovar.wglab.org/

References

1. Shoubridge, E.A. (2001). Nuclear genetic defects of oxidative phosphorylation. Hum. Mol. Genet. *10*, 2277–2284.
2. Park, C.B., and Larsson, N.G. (2011). Mitochondrial DNA mutations in disease and aging. J. Cell Biol. *193*, 809–818.
3. Lightowlers, R.N., Taylor, R.W., and Turnbull, D.M. (2015). Mutations causing mitochondrial disease: What is new and what challenges remain? Science *349*, 1494–1499.
4. Baker, M.J., Frazier, A.E., Gulbis, J.M., and Ryan, M.T. (2007). Mitochondrial protein-import machinery: correlating structure with function. Trends Cell Biol. *17*, 456–464.
5. Mokranjac, D., and Neupert, W. (2009). Thirty years of protein translocation into mitochondria: unexpectedly complex and still puzzling. Biochim. Biophys. Acta *1793*, 33–41.
6. Schmidt, O., Pfanner, N., and Meisinger, C. (2010). Mitochondrial protein import: from proteomics to functional mechanisms. Nat. Rev. Mol. Cell Biol. *11*, 655–667.
7. Herrmann, J.M., and Riemer, J. (2012). Mitochondrial disulfide relay: redox-regulated protein import into the intermembrane space. J. Biol. Chem. *287*, 4426–4433.
8. Vögtle, F.N., Wortelkamp, S., Zahedi, R.P., Becker, D., Leidhold, C., Gevaert, K., Kellermann, J., Voos, W., Sickmann, A., Pfanner, N., and Meisinger, C. (2009). Global analysis of the mitochondrial N-proteome identifies a processing peptidase critical for protein stability. Cell *139*, 428–439.
9. Habib, S.J., Neupert, W., and Rapaport, D. (2007). Analysis and prediction of mitochondrial targeting signals. Methods Cell Biol. *80*, 761–781.
10. Schulz, C., Schendzielorz, A., and Rehling, P. (2015). Unlocking the presequence import pathway. Trends Cell Biol. *25*, 265–275.
11. Taylor, A.B., Smith, B.S., Kitada, S., Kojima, K., Miyaura, H., Otwinowski, Z., Ito, A., and Deisenhofer, J. (2001). Crystal structures of mitochondrial processing peptidase reveal the mode for specific cleavage of import signal sequences. Structure *9*, 615–625.
12. Gakh, O., Cavadini, P., and Isaya, G. (2002). Mitochondrial processing peptidases. Biochim. Biophys. Acta *1592*, 63–77.
13. Kučera, T., Otyepka, M., Matušková, A., Samad, A., Kutejová, E., and Janata, J. (2013). A computational study of the glycine-rich loop of mitochondrial processing peptidase. PLoS ONE *8*, e74518.

14. Quirós, P.M., Langer, T., and López-Otín, C. (2015). New roles for mitochondrial proteases in health, ageing and disease. Nat. Rev. Mol. Cell Biol. *16*, 345–359.
15. Poveda-Huertes, D., Mulica, P., and Vögtle, F.N. (2017). The versatility of the mitochondrial presequence processing machinery: cleavage, quality control and turnover. Cell Tissue Res. *367*, 73–81.
16. Sobreira, N., Schiettecatte, F., Valle, D., and Hamosh, A. (2015). GeneMatcher: a matching tool for connecting investigators with an interest in the same gene. Hum. Mutat. *36*, 928–930.
17. Li, H., and Durbin, R. (2009). Fast and accurate short read alignment with Burrows-Wheeler transform. Bioinformatics *25*, 1754–1760.
18. Li, H., Handsaker, B., Wysoker, A., Fennell, T., Ruan, J., Homer, N., Marth, G., Abecasis, G., Durbin, R.; and 1000 Genome Project Data Processing Subgroup (2009). The Sequence Alignment/Map format and SAMtools. Bioinformatics *25*, 2078–2079.
19. Goecks, J., Nekrutenko, A., Taylor, J.; and Galaxy Team (2010). Galaxy: a comprehensive approach for supporting accessible, reproducible, and transparent computational research in the life sciences. Genome Biol. *11*, R86.
20. Farwell, K.D., Shahmirzadi, L., El-Khechen, D., Powis, Z., Chao, E.C., Tippin Davis, B., Baxter, R.M., Zeng, W., Mroske, C., Parra, M.C., et al. (2015). Enhanced utility of family-centered diagnostic exome sequencing with inheritance model-based analysis: results from 500 unselected families with undiagnosed genetic conditions. Genet. Med. *17*, 578–586.
21. Helbig, K.L., Farwell Hagman, K.D., Shinde, D.N., Mroske, C., Powis, Z., Li, S., Tang, S., and Helbig, I. (2016). Diagnostic exome sequencing provides a molecular diagnosis for a significant proportion of patients with epilepsy. Genet. Med. *18*, 898–905.
22. Miyake, N., Tsukaguchi, H., Koshimizu, E., Shono, A., Matsunaga, S., Shiina, M., Mimura, Y., Imamura, S., Hirose, T., Okudela, K., et al. (2015). Biallelic mutations in nuclear pore complex subunit NUP107 cause early-childhood-onset steroid-resistant nephrotic syndrome. Am. J. Hum. Genet. *97*, 555–566.
23. Fujita, A., Isidor, B., Piloquet, H., Corre, P., Okamoto, N., Nakashima, M., Tsurusaki, Y., Saitsu, H., Miyake, N., and Matsumoto, N. (2016). De novo MEIS2 mutation causes syndromic developmental delay with persistent gastro-esophageal reflux. J. Hum. Genet. *61*, 835–838.
24. Yang, H., and Wang, K. (2015). Genomic variant annotation and prioritization with ANNOVAR and wANNOVAR. Nat. Protoc. *10*, 1556–1566.
25. Suls, A., Jaehn, J.A., Kecskés, A., Weber, Y., Weckhuysen, S., Craiu, D.C., Siekierska, A., Djémié, T., Afrikanova, T., Gormley, P., et al.; EuroEPINOMICS RES Consortium (2013). De novo loss-of-function mutations in CHD2 cause a fever-sensitive myoclonic epileptic encephalopathy sharing features with Dravet syndrome. Am. J. Hum. Genet. *93*, 967–975.
26. Emsley, P., Lohkamp, B., Scott, W.G., and Cowtan, K. (2010). Features and development of Coot. Acta Crystallogr. D Biol. Crystallogr. *66*, 486–501.
27. Bhutani, K., Nazor, K.L., Williams, R., Tran, H., Dai, H., Džakula, Ž., Cho, E.H., Pang, A.W.C., Rao, M., Cao, H., et al. (2016). Whole-genome mutational burden analysis of three pluripotency induction methods. Nat. Commun. *7*, 10536.
28. Merkle, F.T., Ghosh, S., Kamitaki, N., Mitchell, J., Avior, Y., Mello, C., Kashin, S., Mekhoubad, S., Ilic, D., Charlton, M., et al. (2017). Human pluripotent stem cells recurrently acquire and expand dominant negative P53 mutations. Nature *545*, 229–233.
29. Okita, K., Matsumura, Y., Sato, Y., Okada, A., Morizane, A., Okamoto, S., Hong, H., Nakagawa, M., Tanabe, K., Tezuka, K., et al. (2011). A more efficient method to generate integration-free human iPS cells. Nat. Methods *8*, 409–412.
30. Beers, J., Gulbranson, D.R., George, N., Siniscalchi, L.I., Jones, J., Thomson, J.A., and Chen, G. (2012). Passaging and colony expansion of human pluripotent stem cells by enzyme-free dissociation in chemically defined culture conditions. Nat. Protoc. *7*, 2029–2040.
31. Martí, M., Mulero, L., Pardo, C., Morera, C., Carrió, M., Laricchia-Robbio, L., Esteban, C.R., and Izpisua Belmonte, J.C. (2013). Characterization of pluripotent stem cells. Nat. Protoc. *8*, 223–253.
32. Müller, F.-J., Schuldt, B.M., Williams, R., Mason, D., Altun, G., Papapetrou, E.P., Danner, S., Goldmann, J.E., Herbst, A., Schmidt, N.O., et al. (2011). A bioinformatic assay for pluripotency in human cells. Nat. Methods *8*, 315–317.
33. Koch, P., Opitz, T., Steinbeck, J.A., Ladewig, J., and Brüstle, O. (2009). A rosette-type, self-renewing human ES cell-derived neural stem cell with potential for in vitro instruction and synaptic integration. Proc. Natl. Acad. Sci. USA *106*, 3225–3230.
34. Chambers, S.M., Fasano, C.A., Papapetrou, E.P., Tomishima, M., Sadelain, M., and Studer, L. (2009). Highly efficient neural conversion of human ES and iPS cells by dual inhibition of SMAD signaling. Nat. Biotechnol. *27*, 275–280.
35. Steinbeck, J.A., Koch, P., Derouiche, A., and Brüstle, O. (2012). Human embryonic stem cell-derived neurons establish region-specific, long-range projections in the adult brain. Cell. Mol. Life Sci. *69*, 461–470.
36. Meisinger, C., Pfanner, N., and Truscott, K.N. (2006). Isolation of yeast mitochondria. Methods Mol. Biol. *313*, 33–39.
37. Mossmann, D., Vögtle, F.N., Taskin, A.A., Teixeira, P.F., Ring, J., Burkhart, J.M., Burger, N., Pinho, C.M., Tadic, J., Loreth, D., et al. (2014). Amyloid-β peptide induces mitochondrial dysfunction by inhibition of preprotein maturation. Cell Metab. *20*, 662–669.
38. Wiedemann, N., Urzica, E., Guiard, B., Müller, H., Lohaus, C., Meyer, H.E., Ryan, M.T., Meisinger, C., Mühlenhoff, U., Lill, R., and Pfanner, N. (2006). Essential role of Isd11 in mitochondrial iron-sulfur cluster synthesis on Isu scaffold proteins. EMBO J. *25*, 184–195.
39. Chatfield, K.C., Coughlin, C.R., 2nd, Friederich, M.W., Gallagher, R.C., Hesselberth, J.R., Lovell, M.A., Ofman, R., Swanson, M.A., Thomas, J.A., Wanders, R.J., et al. (2015). Mitochondrial energy failure in HSD10 disease is due to defective mtDNA transcript processing. Mitochondrion *21*, 1–10.
40. Coughlin, C.R., 2nd, Scharer, G.H., Friederich, M.W., Yu, H.-C., Geiger, E.A., Creadon-Swindell, G., Collins, A.E., Vanlander, A.V., Coster, R.V., Powell, C.A., et al. (2015). Mutations in the mitochondrial cysteinyl-tRNA synthase gene, *CARS2*, lead to a severe epileptic encephalopathy and complex movement disorder. J. Med. Genet. *52*, 532–540.

41. Friederich, M.W., Erdogan, A.J., Coughlin, C.R., 2nd, Elos, M.T., Jiang, H., O'Rourke, C.P., Lovell, M.A., Wartchow, E., Gowan, K., Chatfield, K.C., et al. (2017). Mutations in the accessory subunit NDUFB10 result in isolated complex I deficiency and illustrate the critical role of intermembrane space import for complex I holoenzyme assembly. Hum. Mol. Genet. *26*, 702–716.
42. Vogel, R.O., Smeitink, J.A., and Nijtmans, L.G. (2007). Human mitochondrial complex I assembly: a dynamic and versatile process. Biochim. Biophys. Acta *1767*, 1215–1227.
43. Condò, I., Malisan, F., Guccini, I., Serio, D., Rufini, A., and Testi, R. (2010). Molecular control of the cytosolic aconitase/IRP1 switch by extramitochondrial frataxin. Hum. Mol. Genet. *19*, 1221–1229.
44. Tong, W.-H., and Rouault, T.A. (2006). Functions of mitochondrial ISCU and cytosolic ISCU in mammalian iron-sulfur cluster biogenesis and iron homeostasis. Cell Metab. *3*, 199–210.
45. Baker, P.R., 2nd, Friederich, M.W., Swanson, M.A., Shaikh, T., Bhattacharya, K., Scharer, G.H., Aicher, J., Creadon-Swindell, G., Geiger, E., MacLean, K.N., et al. (2014). Variant non ketotic hyperglycinemia is caused by mutations in LIAS, BOLA3 and the novel gene GLRX5. Brain *137*, 366–379.
46. Cavadini, P., Adamec, J., Taroni, F., Gakh, O., and Isaya, G. (2000). Two-step processing of human frataxin by mitochondrial processing peptidase. Precursor and intermediate forms are cleaved at different rates. J. Biol. Chem. *275*, 41469–41475.
47. Schmucker, S., Argentini, M., Carelle-Calmels, N., Martelli, A., and Puccio, H. (2008). The in vivo mitochondrial two-step maturation of human frataxin. Hum. Mol. Genet. *17*, 3521–3531.
48. Lill, R., Srinivasan, V., and Mühlenhoff, U. (2014). The role of mitochondria in cytosolic-nuclear iron–sulfur protein biogenesis and in cellular iron regulation. Curr. Opin. Microbiol. *22*, 111–119.
49. Braymer, J.J., and Lill, R. (2017). Iron-sulfur cluster biogenesis and trafficking in mitochondria. J. Biol. Chem. *292*, 12754–12763.
50. Rouault, T.A., and Maio, N. (2017). Biogenesis and functions of mammalian iron-sulfur proteins in the regulation of iron homeostasis and pivotal metabolic pathways. J. Biol. Chem. *292*, 12744–12753.
51. Gakh, O., Bedekovics, T., Duncan, S.F., Smith, D.Y., 4th, Berkholz, D.S., and Isaya, G. (2010). Normal and Friedreich ataxia cells express different isoforms of frataxin with complementary roles in iron-sulfur cluster assembly. J. Biol. Chem. *285*, 38486–38501.
52. Fox, N.G., Das, D., Chakrabarti, M., Lindahl, P.A., and Barondeau, D.P. (2015). Frataxin accelerates [2Fe-2S] cluster formation on the human Fe-S assembly complex. Biochemistry *54*, 3880–3889.
53. Xu, X., Duan, S., Yi, F., Ocampo, A., Liu, G.H., and Izpisua Belmonte, J.C. (2013). Mitochondrial regulation in pluripotent stem cells. Cell Metab. *18*, 325–332.
54. Witte, C., Jensen, R.E., Yaffe, M.P., and Schatz, G. (1988). MAS1, a gene essential for yeast mitochondrial assembly, encodes a subunit of the mitochondrial processing protease. EMBO J. *7*, 1439–1447.
55. Burkhart, J.M., Taskin, A.A., Zahedi, R.P., and Vögtle, F.N. (2015). Quantitative profiling for substrates of the mitochondrial presequence processing protease reveals a set of nonsubstrate proteins increased upon proteotoxic stress. J. Proteome Res. *14*, 4550–4563.
56. Mick, D.U., Fox, T.D., and Rehling, P. (2011). Inventory control: cytochrome c oxidase assembly regulates mitochondrial translation. Nat. Rev. Mol. Cell Biol. *12*, 14–20.
57. Wittig, I., Braun, H.P., and Schägger, H. (2006). Blue native PAGE. Nat. Protoc. *1*, 418–428.
58. Stuart, R.A. (2008). Supercomplex organization of the oxidative phosphorylation enzymes in yeast mitochondria. J. Bioenerg. Biomembr. *40*, 411–417.
59. Jobling, R.K., Assoum, M., Gakh, O., Blaser, S., Raiman, J.A., Mignot, C., Roze, E., Dürr, A., Brice, A., Lévy, N., et al. (2015). PMPCA mutations cause abnormal mitochondrial protein processing in patients with non-progressive cerebellar ataxia. Brain *138*, 1505–1517.
60. Choquet, K., Zurita-Rendón, O., La Piana, R., Yang, S., Dicaire, M.J., Boycott, K.M., Majewski, J., Shoubridge, E.A., Brais, B., Tétreault, M.; and Care4Rare Consortium (2016). Autosomal recessive cerebellar ataxia caused by a homozygous mutation in PMPCA. Brain *139*, e19.
61. Joshi, M., Anselm, I., Shi, J., Bale, T.A., Towne, M., Schmitz-Abe, K., Crowley, L., Giani, F.C., Kazerounian, S., Markianos, K., et al. (2016). Mutations in the substrate binding glycine-rich loop of the mitochondrial processing peptidase-α protein (PMPCA) cause a severe mitochondrial disease. Cold Spring Harb. Mol. Case Stud. *2*, a000786.
62. Isaya, G. (2014). Mitochondrial iron-sulfur cluster dysfunction in neurodegenerative disease. Front. Pharmacol. *5*, 29.
63. Muthuswamy, S., and Agarwal, S. (2015). Friedreich ataxia: from the eye of a molecular biologist. Neurologist *20*, 51–55.
64. Campuzano, V., Montermini, L., Moltò, M.D., Pianese, L., Cossée, M., Cavalcanti, F., Monros, E., Rodius, F., Duclos, F., Monticelli, A., et al. (1996). Friedreich's ataxia: autosomal recessive disease caused by an intronic GAA triplet repeat expansion. Science *271*, 1423–1427.
65. Nizon, M., Boutron, A., Boddaert, N., Slama, A., Delpech, H., Sardet, C., Brassier, A., Habarou, F., Delahodde, A., Correia, I., et al. (2014). Leukoencephalopathy with cysts and hyperglycinemia may result from NFU1 deficiency. Mitochondrion *15*, 59–64.
66. Lebigot, E., Gaignard, P., Dorboz, I., Slama, A., Rio, M., de Lonlay, P., Héron, B., Sabourdy, F., Boespflug-Tanguy, O., Cardoso, A., et al. (2017). Impact of mutations within the [Fe-S] cluster or the lipoic acid biosynthesis pathways on mitochondrial protein expression profiles in fibroblasts from patients. Mol. Genet. Metab. *122*, 85–94, Epub ahead of print.
67. Ahting, U., Mayr, J.A., Vanlander, A.V., Hardy, S.A., Santra, S., Makowski, C., Alston, C.L., Zimmermann, F.A., Abela, L., Plecko, B., et al. (2015). Clinical, biochemical, and genetic spectrum of seven patients with NFU1 deficiency. Front. Genet. *6*, 123.
68. Haack, T.B., Rolinski, B., Haberberger, B., Zimmermann, F., Schum, J., Strecker, V., Graf, E., Athing, U., Hoppen, T., Wittig, I., et al. (2013). Homozygous missense mutation in BOLA3 causes multiple mitochondrial dysfunctions syndrome in two siblings. J. Inherit. Metab. Dis. *36*, 55–62.
69. Debray, F.-G., Stümpfig, C., Vanlander, A.V., Dideberg, V., Josse, C., Caberg, J.H., Boemer, F., Bours, V., Stevens, R., Seneca, S., et al. (2015). Mutation of the iron-sulfur cluster assembly gene *IBA57* causes fatal infantile leukodystrophy. J. Inherit. Metab. Dis. *38*, 1147–1153.

70. Farhan, S.M.K., Wang, J., Robinson, J.F., Lahiry, P., Siu, V.M., Prasad, C., Kronick, J.B., Ramsay, D.A., Rupar, C.A., and Hegele, R.A. (2014). Exome sequencing identifies NFS1 deficiency in a novel Fe-S cluster disease, infantile mitochondrial complex II/III deficiency. Mol. Genet. Genomic Med. *2*, 73–80.
71. Mochel, F., Knight, M.A., Tong, W.H., Hernandez, D., Ayyad, K., Taivassalo, T., Andersen, P.M., Singleton, A., Rouault, T.A., Fischbeck, K.H., and Haller, R.G. (2008). Splice mutation in the iron-sulfur cluster scaffold protein ISCU causes myopathy with exercise intolerance. Am. J. Hum. Genet. *82*, 652–660.
72. Guo, R., Zong, S., Wu, M., Gu, J., and Yang, M. (2017). Architecture of human mitochondrial respiratory megacomplex $I_2III_2IV_2$. Cell *170*, 1247–1257.e12.
73. Rötig, A., de Lonlay, P., Chretien, D., Foury, F., Koenig, M., Sidi, D., Munnich, A., and Rustin, P. (1997). Aconitase and mitochondrial iron-sulphur protein deficiency in Friedreich ataxia. Nat. Genet. *17*, 215–217.